ACS Energy LETTERS

Cite This: ACS Energy Lett. 2018, 3, 546−554

LETTER

Trimetallic NiFeMo for Overall Electrochemical Water Splitting with a Low Cell Voltage

Fan Qin,[†] Zhenhuan Zhao,[‡,#] Md Kamrul Alam,[†] Yizhou Ni,[∥] Francisco Robles-Hernandez,[#,§] Luo Yu,[∥] Shuo Chen,[∥] Zhifeng Ren,[∥] Zhiming Wang,[‡] and Jiming Bao*[,†,‡,#]

[†]Materials Science & Engineering, University of Houston, Houston, Texas 77204, United States

[‡]Institute of Fundamental and Frontier Sciences, University of Electronic Science and Technology of China, Chengdu 610054, China

[#]Department of Electrical and Computer Engineering, University of Houston, Houston, Texas 77204, United States

[∥]Department of Physics & The Texas Center for Superconductivity, University of Houston, Houston, Texas 77204, United States

[§]College of Technology, University of Houston, Houston, Texas 77204, United States

Supporting Information

ABSTRACT: We report the development of an efficient and earth-abundant catalyst for electrochemical overall water splitting. Trimetallic NiFeMo alloy is synthesized by hydrothermal deposition from inorganic precursors and subsequent low-temperature thermal annealing. A complete cell made of NiFeMo electrodes on nickel foam exhibits a low voltage of 1.45 V at 10 mA/cm^2 as a result of low overpotentials for both hydrogen evolution reaction (HER) and oxygen evolution reaction (OER). High-resolution transmission electron microscopy reveals that nanometer-sized single-crystal domains of Ni, Fe, and Mo are intimately integrated at the atomic level, which enables a synergistic effect of metallic Ni, Fe, and Mo for efficient HER, while self-formed Ni−Fe−Mo (oxy)hydroxides on the surface of the NiFeMo anode become active sites for OER. Such a multimetallic alloy and its (oxy)hydroxides represent a typical HER/OER catalyst couple, and our method provides a new route to develop efficient low-cost metallic alloys for overall water splitting.

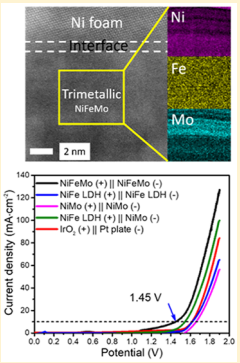

Electrochemical water splitting into hydrogen fuel and oxygen using solar energy is a clean and sustainable technique that cannot only meet the world's potential energy demand but also reduce greenhouse gas emission. It becomes even more important today because solar electricity generation from photovoltaics and wind farms has been mature and commercially employed with an ever-increasing capacity.[1−3] Because the core components of efficient water splitting cells are materials that should catalyze hydrogen evolution reaction (HER) and oxygen evolution reaction (OER) at low cost for a long period, there have been great efforts to develop highly active catalysts based on earth-abundant elements.[4,5] Among them, overall water-splitting catalysts that can perform both HER and OER are particularly appealing because of the simplicity in implementing the system where only one type of electrolyte and electrode are needed.[6] Past years have witnessed the emergence of catalysts with various elemental compositions and structures, but large cell voltages (>1.5 V, defined at the current density of 10 mA cm^{-2}) are usually required.[6−27] More active catalysts with lower cell voltages and other better characteristics are needed in order to make water electrolysis economically viable.[28−30] Note that well-designed nanostructures have played an important role in increasing current density and reducing the cell voltages, but they suffer from complicated synthesis and low yields.[7,10,15,22,25,31]

An efficient water-splitting catalyst must exhibit excellent performance for both HER and OER; therefore, it is more challenging to design and fabricate than a HER or OER catalyst alone. For example, Pt is the best HER catalyst, but IrO_2 is much better for OER.[1] Stability is another serious issue. Most above-mentioned catalysts such as metal sulfides,[26,32,33] selenides,[8,9] and phosphides,[10−12,14,19,24] become partially or entirely converted to the metal oxides/(oxy)hydroxides accompanied by the dissolution of anionic elements under a high oxidation potential in the electrolyte.[34]

The ternary Ni−Mo−Fe composites have been reported as HER and OER electrocatalysts in an alkaline electrolyte. For the HER, the Ni−Mo−Fe alloy composite shows huge potential for industrial hydrogen production. However, the previously reported Ni−Mo−Fe HER electrocatalysts usually show different compositions or atomic ratios,[35−40] and the most active composition is still not clear while the OER performance of the reported Ni−Mo−Fe needs to be improved. For example, the most recent work prepared

Received: December 25, 2017
Accepted: February 6, 2018
Published: February 6, 2018

DOI: 10.1021/acsenergylett.7b01335
ACS Energy Lett. 2018, 3, 546−554

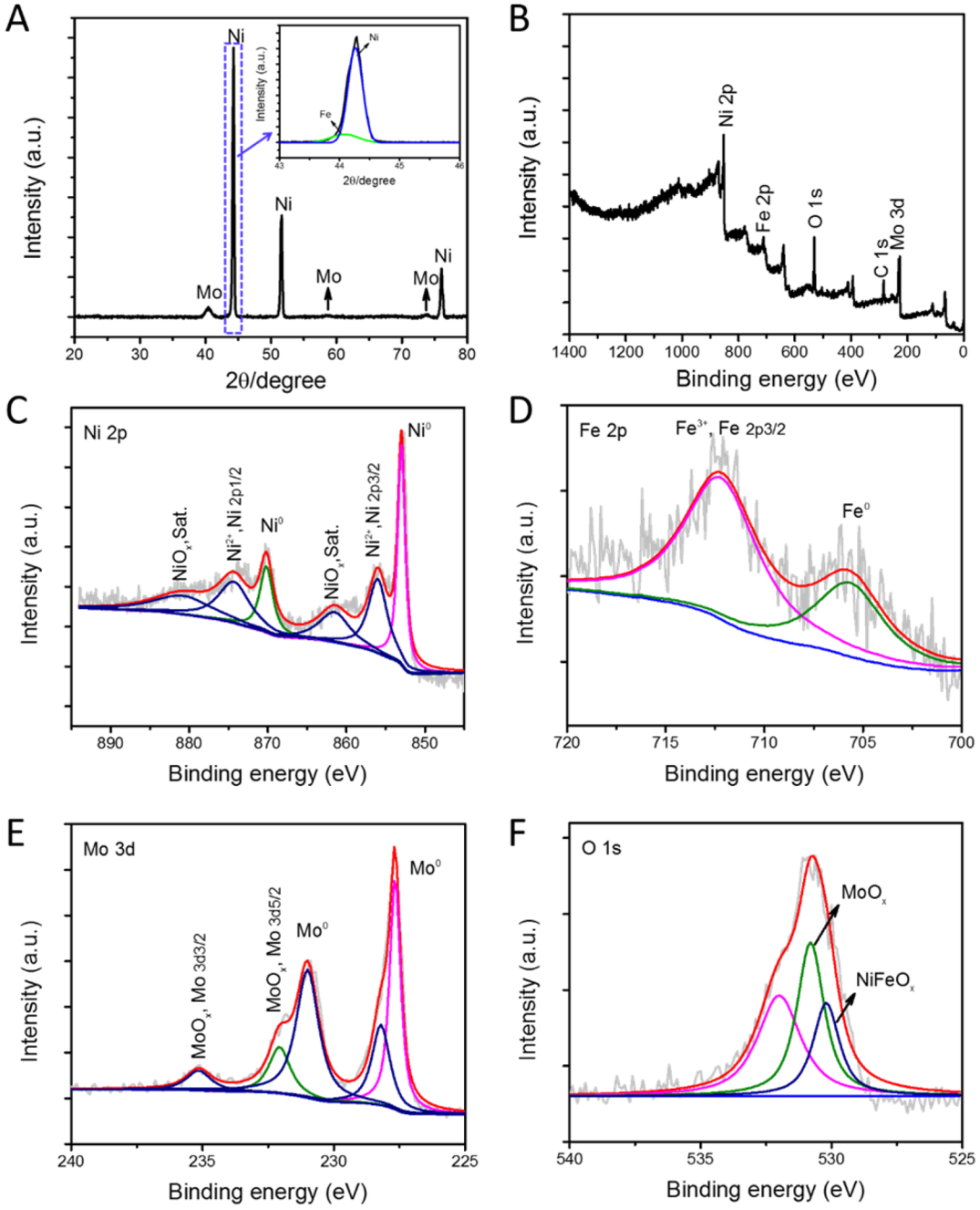

Figure 1. Chemical composition characterizations by XRD and XPS spectroscopy of a NiFeMo film on Ni foam. (A) XRD pattern, standard data: Ni (JCPDS No. 65-380), Fe (JCPDS No. 1-1252), and Mo (JCPDS No. 1-1205). (B) XPS elemental survey. (C–F) XPS high-resolution scans of (C) Ni 2p, (D) Fe 2p, (E) Mo 3d, and (F) O 1s.

MoO^{4-} intercalated NiFe layered double hydroxide (LDH), but large overpotentials are still required (η_{10} > 270 mV).[41,42] Up to now, quite a few studies report the HER and OER activities on a single electrode;[43,44] therefore, it is highly significant to optimize the trimetallic Ni–Fe–Mo system for overall water splitting. Here we reported a trimetallic NiFeMo thin film on Ni foam synthesized by hydrothermal deposition and H_2-induced alloying. This straightforward approach leads to the combination of a Ni–Mo and Ni–Fe catalyst that yields high practical HER and OER activity with no need to optimize catalyst components independently. This binder-free water-splitting catalyst served as the HER catalyst and the precatalyst for the OER catalyst, and the NiFeMo(−)||NiFeMo(+) couple exhibited a cell voltage of as low as 1.45 V in alkaline solution.

To fabricate binder-free NiFeMo catalyst, we first immersed nickel foam in an aqueous solution of $NiCl_2{\cdot}6H_2O$, $FeCl_3{\cdot}6H_2O$, and Na_2MoO_4 with a molar ratio of 1:1:2 in an autoclave at 160 °C for 6 h. The foam was then taken out and annealed in a forming gas of Ar/H_2 at 500 °C for 1 h. Other trimetallic or bimetallic samples such as NiFe, FeMo, and NiMo were also fabricated with a similar process. More details are provided in the experimental section of the Supporting Information. The X-ray diffraction (XRD) pattern in Figure 1A shows the appearance of Fe and Mo peaks besides stronger Ni lines. The coexistence of Fe, Mo, and Ni is also confirmed by X-

DOI: 10.1021/acsenergylett.7b01335
ACS Energy Lett. 2018, 3, 546–554

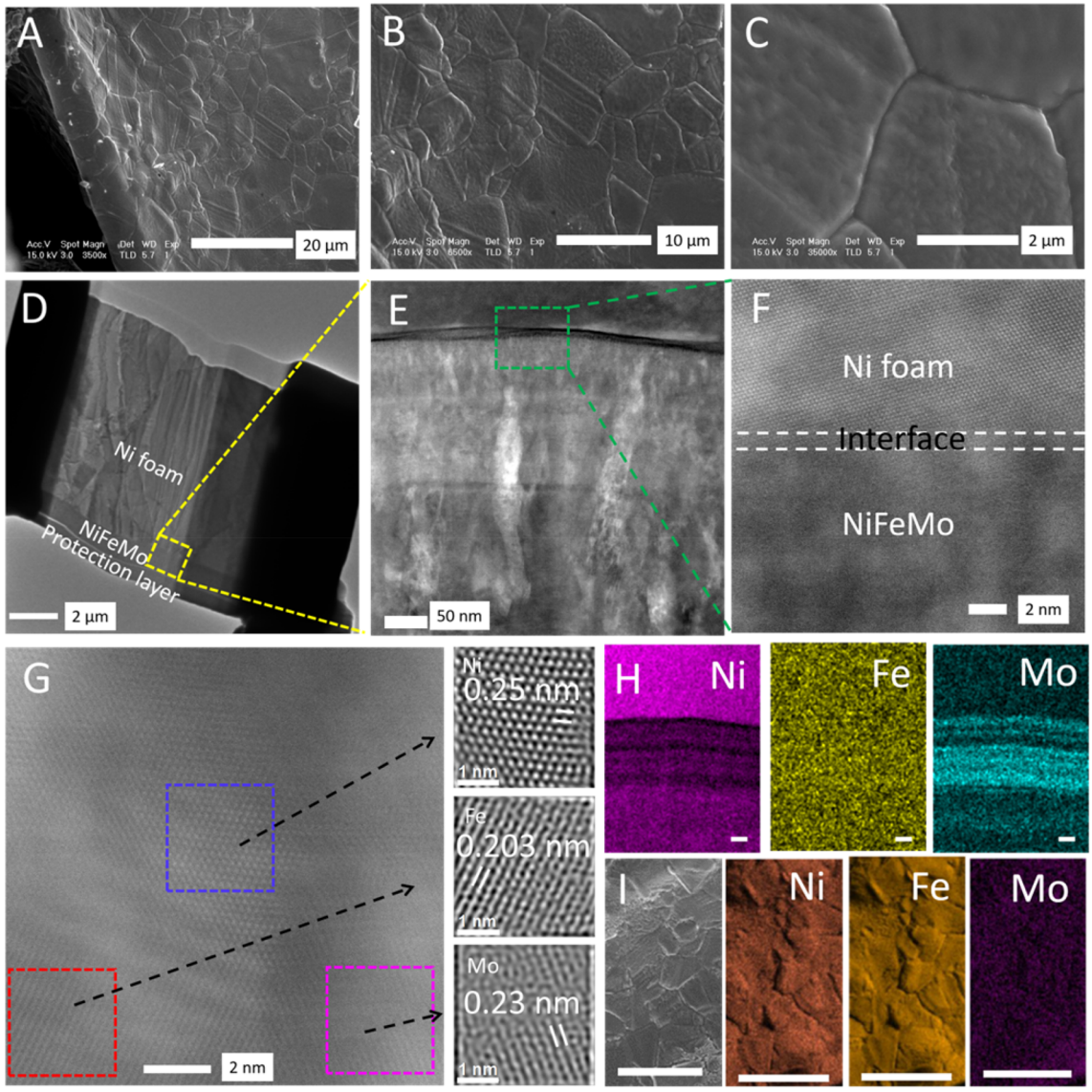

Figure 2. Morphology and lattice structure of NiFeMo. (A–C) SEM images of the NiFeMo film. (D,E) TEM images of a cross section prepared by FIB. (F,G) High-resolution TEM images. (H) EDS elemental mapping images from TEM; scale bars: 50 nm. (I) Surface SEM and EDS elemental mapping images; scale bar: 100 μm.

ray photoelectron spectroscopy (XPS) in Figure 1B. Metallic Ni, Fe, and Mo signatures can be seen from the detailed XPS spectra in Figure 1C–F besides their oxides due to exposure to air. Due to the difficulty in distinguishing the metallic Ni signal from the Ni foam substrate and deposited metallic Ni, the NiFeMo film was deposited onto Cu foam through the same process to obtain an accurate atomic ratio of the three metals. The corresponding XPS results in Figure S1 (Supporting Information) indicate the formation of trimetallic NiFeMo, and the relative intensity gives us the atomic ratio of Ni, Fe, and Mo to be 1:1.34:2.18.

Scanning electron microscopy (SEM) images in Figure 2A–C indicate that Ni foam (Figure S2, Supporting Information) is still covered by a smooth and compact film. To find out the thickness of the film and spatial distribution of Fe, Mo, and Ni, we used focused ion beam (FIB) to cut out a cross-sectional piece (Figure S3, Supporting Information) and studied it with transmission electron microscopy (TEM). High resolution TEM images in Figure 2D–G confirm that the NiFeMo film is crystalline with mixed nanodomains of Ni, Fe, and Mo. The thickness of the film is about 1 μm. The energy-dispersive X-ray spectroscopy (EDS) elemental mapping in Figure 2H shows a relatively uniform distribution of Ni, Fe, and Mo, which is also confirmed by surface EDS elemental mapping from SEM in Figure 2I, as well as EDS elemental mapping of a scratched flake from TEM in Figure S4 (Supporting Information). For comparison, a series of alloys with different Ni, Fe, and Mo ratios were prepared. The SEM images (Figure S5, Supporting Information) indicate that they have a similar film morphology but different surface roughness. Moreover, a compact film is observed for bimetallic NiFe and FeMo (Figure S6A–D, Supporting Information), but the NiMo alloy (Figure S6E,F, Supporting Information) forms a uniform nanowire structure, consistent with the literature.[45]

HER, OER, and overall water splitting were evaluated in N_2-saturated 1.0 M KOH aqueous solution—a typical water-splitting electrolyte. The Ag/AgCl electrode and Pt wire were used as the reference and counter electrodes, respectively.

DOI: 10.1021/acsenergylett.7b01335
ACS Energy Lett. 2018, 3, 546–554

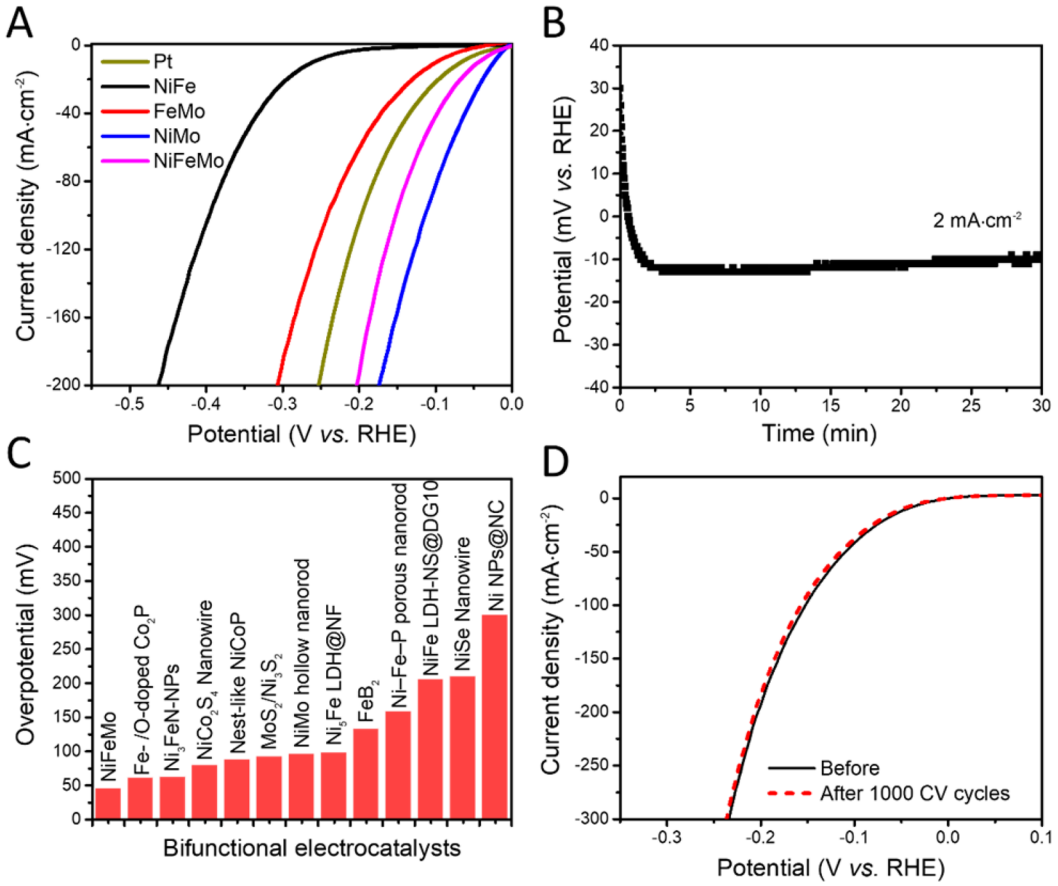

Figure 3. HER performance of Pt plate, NiFe, FeMo, NiMo, and NiFeMo conducted in 1.0 M KOH. (A) Polarization curves and (B) onset HER potential. (C) Comparison with selected state-of-art water-splitting electrocatalysts. (D) Polarization curves of the NiFeMo before and after 1000 CV cycles. References cited in (C): Fe-/O-doped Co_2P,[48] Ni_3FeN-NPs,[49] $NiCo_2S_4$ nanowire,[26] nest-like NiCoP,[12] MoS_2/Ni_3S_2,[32] NiMo hollow nanorod,[25] Ni_5Fe LDH@NF,[20] FeB_2,[16] Ni–Fe–P,[50] NiFe LDH-NS@DG-10,[51] NiSe nanowire,[9] and Ni NPs@NC.[52]

Potentials reported in this work are referenced to the reversible hydrogen electrode (RHE), and the polarization curves are corrected against the ohmic potential drop (Figure S7, Supporting Information). The catalytic performances of NiFeMo samples synthesized with different $NiCl_2{\cdot}6H_2O$, $FeCl_3{\cdot}6H_2O$, and Na_2MoO_4 ratios were first studied, and NiFeMo with an initial molar ratio of 1:1:2 exhibited the best catalytic activity in both HER and OER; further increase in Mo molar ratio had little effect on the activity (Figure S8, Supporting Information). Unless otherwise stated, NiFeMo is referred to as the sample with this optimal 1:1:2 ratio. Figure 3A shows HER polarization curves of the NiFeMo and two bimetallic samples. The NiFeMo exhibits a low overpotential η_{10} of 45 mV, which is significantly lower than that of the control samples (262 mV for NiFe, 100 mV for FeMo, and 68 mV for Pt plate). An ultrasmall onset potential of 12 mV is observed for the NiFeMo film (Figure 3B). Figure 3C plots recently reported water-splitting catalysts based on their overpotential at a geometric current density of 10 mA cm^{-2}, with NiFeMo having a comparable overpotential. Furthermore, we also summarized recent reported HER catalysts (Table S1, Supporting Information); NiFeMo exhibits a comparable or even better catalytic performance among the best catalysts. Note that the flat Pt plate has smaller surface area than the Ni foam, indicating that the surface area effect should be an important reason for the difference in activity of the NiFeMo film compared to that of the Pt plate. Meanwhile, the NiMo alloy exhibits a lower overpotential, but its specific nanowire structure makes it difficult to compare with other film samples; more comparisons will be discussed in the following text.

To gain more insight into the HER activity of NiFeMo, we performed electrochemical impedance spectroscopy (EIS). The Nyquist plots in Figure S9 (Supporting Information) show a single semicircle without Warburg impedance in the low-frequency range for each catalyst, suggesting a rapid mass transport process and a kinetically controlled reaction.[46] The NiFeMo exhibits charge-transfer resistance R_{ct} of 4.5 Ω. The turnover frequency (TOF, Supporting Information) is calculated to be 0.09 and 0.21 H_2 s^{-1} at η of 100 and 150 mV, respectively. This value is higher than those of reported HER catalysts such as Ni–Mo nanopowder (0.05 H_2 s^{-1})[29] and Ni_2P nanoparticles (0.012 H_2 s^{-1}).[47] To probe the durability of the NiFeMo catalyst, continuous cyclic voltammetry (CV) scan was performed between 0 to 0.15 V (vs RHE) at a 100 mV s^{-1} scan rate. As observed in Figure 3D, the polarization curve remains the same after 1000 CV cycles, indicating its high stability.

Besides the excellent HER activity, trimetallic NiFeMo is also highly active for OER in the same electrolyte; it exhibits the lower overpotential (238 mV, Figure 4A) and the smaller Tafel slope (35 mV dec^{-1}, Figure 4B) among control samples. This performance is comparable with that of reported water-splitting electrocatalysts as well as the OER catalysts summarized in Figure 4C and Table S2 (Supporting Information). The control electrode of the NiFe alloy shows relatively poorer OER activity

DOI: 10.1021/acsenergylett.7b01335
ACS Energy Lett. 2018, 3, 546–554

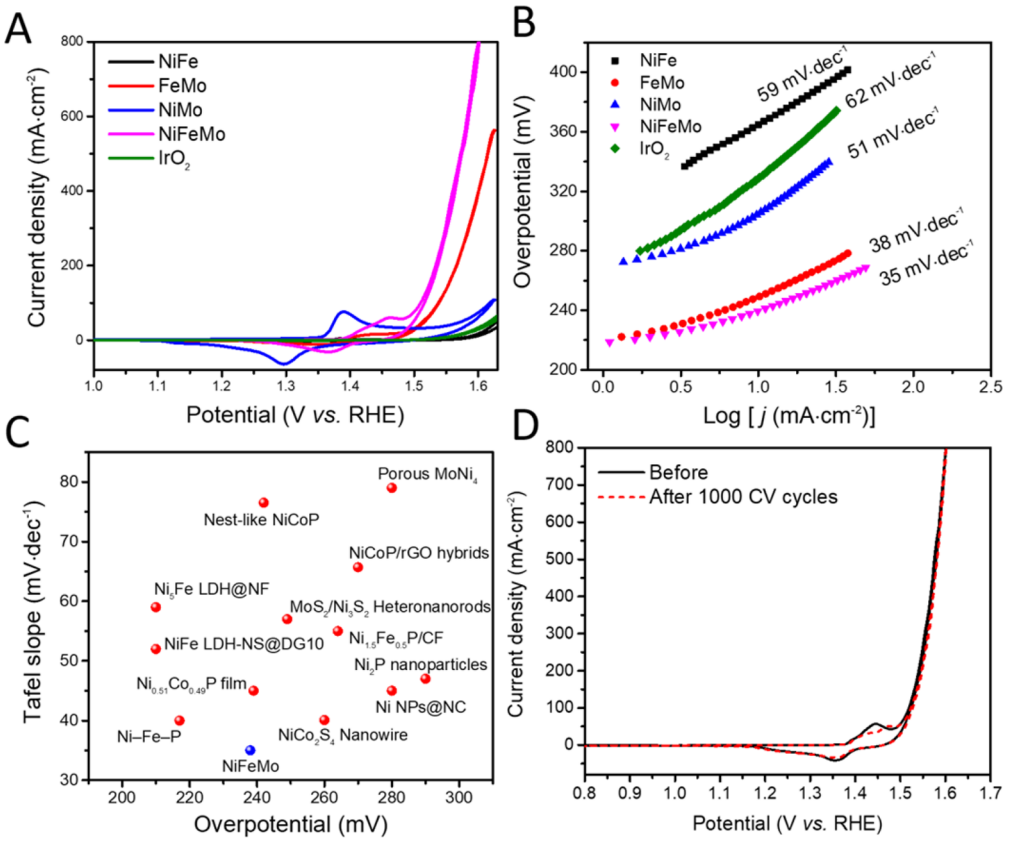

Figure 4. OER performance of NiFe, FeMo, NiMo, NiFeMo, and IrO_2 conducted in 1.0 M KOH. (A) CV curves and (B) Tafel plots. (C) Comparison with selected state-of-art water-splitting electrocatalysts. (D) Polarization curves of the NiFeMo electrocatalyst before and after 1000 CV cycles. References cited in (C): Ni−Fe−P,[50] $NiCo_2S_4$ nanowire,[26] Ni NPs/NC,[52] $Ni_{0.51}Co_{0.49}P$ film,[17] Ni_2P nanoparticles,[24] NiFe LDH-NS@DG10,[51] $Ni_{1.5}Fe_{0.5}P/CF$,[19] MoS_2/Ni_3S_2 heteronanorods,[58] Ni_5Fe LDH@NF,[20] NiCoP/rGO hybrids,[10] nest NiCoP,[12] and porous $MoNi_4$.[18]

than that of other catalysts in the literature,[6] and the reason is probably the difference in the samples' preparation. Our NiFe alloy prepared at a temperature of 160 °C shows a film structure rather than nanosheets prepared at around 120 °C.[6,53] NiFe LDH, one of the most active and benchmarked OER catalysts, was also grown on the same nickel foam at 120 °C for a fair OER comparison later (Figure S10, Supporting Information). The electrochemical double-layer capacitance (C_{dl}) was also measured to investigate the electrochemically active surface area (ECSA, Figure S11, Supporting Information). As revealed in Figure S11E, the NiFeMo possesses the highest C_{dl} (75 mF cm^{-2}), which is ~22 times larger than that of sample NiFe (3.3 mF cm^{-2}). Even though the double-layer capacitance was commonly used for determining the ECSA, this approach is limited, especially for most low-conductive metal oxide OER catalysts. Furthermore, the C_{dl} will also be influenced by other factors such as surface coordination of ions, ion intercalation, chemical capacitance due to the population of trap states, and capacitance from any residual charge-transfer processes in the putative nonfaradaic region.[54−57] Therefore, the ECSA may not reflect the real surface area of the electrodes. In Figure S12 (Supporting Information), the Nyquist plots indicate that the NiFeMo has lower charge-transfer resistance, which means faster OER kinetics. Furthermore, the NiFeMo also exhibited remarkable OER stability, as evidenced by the almost overlapping CV curves (Figure 4D) after 1000 CV cycles.

The polarization curves normalized with ECSA and the loading mass were also compared. Figure S13A,B shows the ECSA normalized HER and OER polarization curves. NiMo shows better HER than NiFeMo, while NiFeMo and FeMo have similar OER when normalized with ECSA. However, as we mentioned above, the ECSA may not reflect the real surface area of the electrodes; therefore, this method may not reflect the real intrinsic activity trend. The mass-specific activities were illustrated in Figures S13C,D and S14 and Table S3: the trimetallic NiFeMo shows the highest activities for both HER and OER.

The excellent HER and OER allow us to build a complete cell with NiFeMo as both the anode and cathode in the same electrolyte. Not surprisingly, the NiFeMo cell exhibits the lowest voltage of 1.45 V among control couples including NiMo||NiMo (1.66 V), NiFe LDH||NiFe LDH (1.62 V), NiFe LDH||NiMo (1.55 V), and IrO_2||Pt plate (1.62 V), as shown in Figure 5A. Moreover, it is notable that the NiFeMo catalyst exhibits a lower or comparable cell voltage compared to the recent reported non-noble metal water-splitting catalysts (Figure 5C). Furthermore, the electrolytic cell demonstrates excellent stability in a prolonged chronoamperometric test at 1.6 V for 50 h (Figure 5B). The durability of the NiFeMo electrode is further supported by the nearly overlapped polarization curves before and after electrolysis (Figure 5D). The stability is also tested in an industrial concentrated electrolyte (7 M KOH under 50 °C), as shown in Figure S15 (Supporting Information). Even though the current density

DOI: 10.1021/acsenergylett.7b01335
ACS Energy Lett. 2018, 3, 546−554

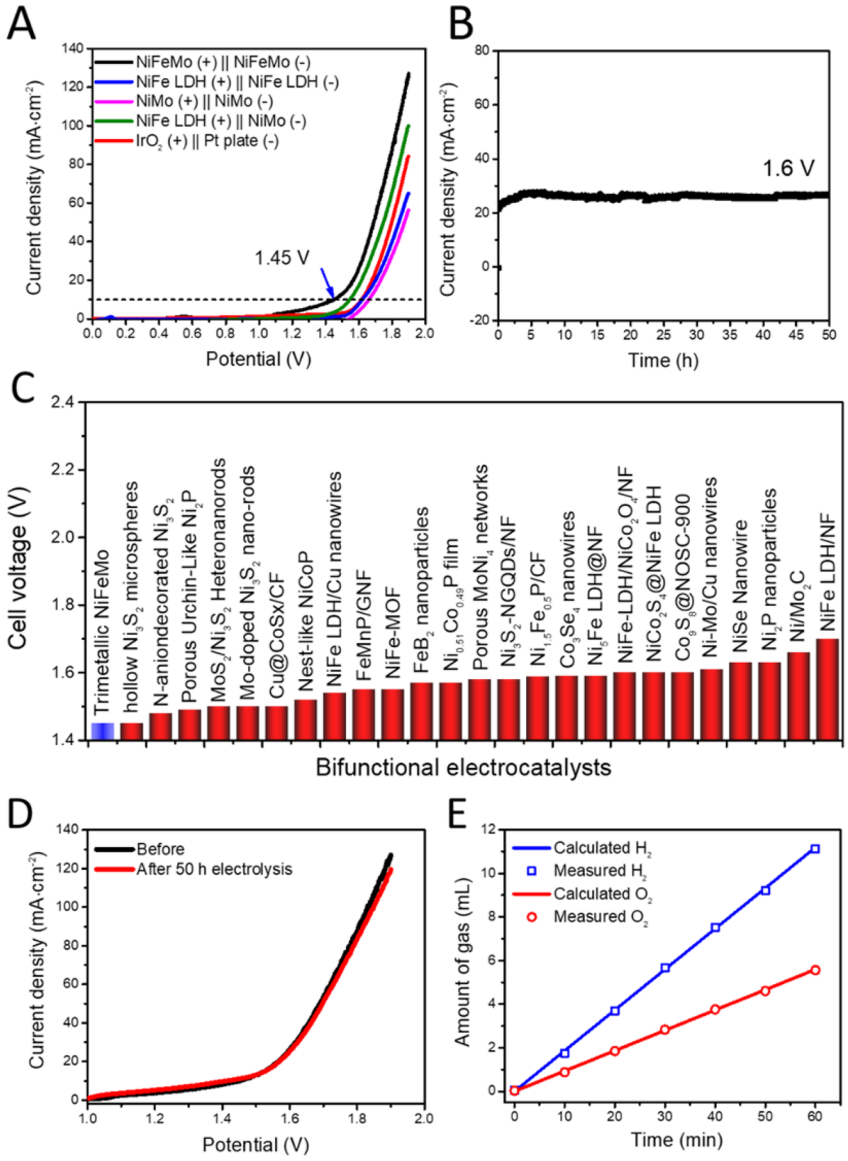

Figure 5. Overall water-splitting performance and stability test of the trimetallic NiFeMo conducted in 1.0 M KOH. (A) Polarization curve for overall water splitting with the NiFeMo electrode as both the anode and cathode at a scan rate of 5 mV s^{-1}. (B) Long-term stability test under an applied voltage of 1.6 V. (C) Comparison of the required cell voltage at 10 mA cm^{-2} of NiFeMo with recently reported noble-metal-free water-splitting electrocatalysts. (D) Polarization curves of before and after 50 h of electrolysis. (E) Amount of gas calculated and experimentally measured along reaction time for overall water splitting of NiFeMo. References cited in (C): Hollow Ni_3S_2 microspheres,[59] N-anion-decorated Ni_3S_2,[60] porous urchin-like Ni_2P,[61] MoS_2/Ni_3S_2 heteronanorods,[58] Mo-doped Ni_3S_2 nanorods,[33] Cu@CoS_x/CF,[62] nest-like NiCoP,[12] NiFe LDH/Cu nanowire,[13] FeMnP/GNF,[14] NiFe-MOF,[15] FeB_2 nanoparticles,[16] $Ni_{0.51}Co_{0.49}P$ film,[17] porous $MoNi_4$ networks,[18] Ni_3S_2−NGQD/NF,[7] $Ni_{1.5}Fe_{0.5}P$/CF,[19] Co_3Se_4 nanowires,[8] Ni_5Fe LDH@NF,[20] NiFe LDH/$NiCo_2O_4$/NF,[27] $NiCo_2S_4$@NiFe LDH,[21] Co_9S_8@NOSC-900,[22] Ni−Mo/Cu nanowires,[23] NiSe nanowire,[9] Ni_2P nanoparticles,[24] Ni/Mo_2C,[63] and NiFe LDH/NF.[6] NF: Ni foam; GNF: graphene/Ni foam; CF: carbon fiber; LDH: layered double hydroxide; NOSC: N-, O-, and S-tridoped carbon-encapsulated.

gradually decreased over the time, the current density could still remain at ∼43 mA·cm^{-2} after 80 h of electrolysis. The Mo concentration in the electrolyte was measured by Inductively coupled plasma optical emission spectrometry (ICP-OES), and the etching rate of Mo was found to be 0.158 $\mu g \cdot g^{-1} \cdot h^{-1}$. We also measured the Faradaic efficiency under controlled potential electrolysis for 60 min. As illustrated in Figure 5E, the actual detected H_2 and O_2 volume along the reaction time is well fitted with the volume calculated from charge transfer, indicating a near-100% Faradaic efficiency.

The challenge of reducing the cell voltage of water-splitting catalysts is that very few materials exhibit both excellent HER and OER in the same electrolyte.[6,25,64] Conventional wisedom is to combine HER and OER catalysts, for example, by growing OER Ni−Fe LDH nanosheets on HER graphene,[51] or synthesizing an OER amorphous Ni−Co complex on HER 1T MoS_2.[33] Such an approach requires an additional complex nanofabrication step; furthermore, it is not clear whether cells with water-splitting catalysts will outperform those with the original separate HER and OER catalysts. Note that no nanofabrication is required for the NiFeMo thin film. Besides its high conductivity and intimate integration with the nickel substrate, a synergistic effect between Ni, Fe, and Mo is responsible for the enhanced HER, which is a function of M−H (metal hydride) bond strength.[1] Because Ni and Fe have a relatively weaker M−H bond strength compared with Mo,[65] a

DOI: 10.1021/acsenergylett.7b01335
ACS Energy Lett. 2018, 3, 546−554

combination of a M−H−weak metal (Ni) with an M−H−strong metal (Mo) can result in an optimized hydrogen adsorption free energy.[66] Although this synergistic effect cannot be directly verified, the identification of metallic elements as active sites for HER is supported by the observation that morphology and the metallic nature of the film remained almost the same after the HER stability test (Figure S16).

According to the characterization results of the sample after OER in Figure S17, SEM images reveal that the nanosheet structure is on the entire surface of the electrode. On the other hand, obvious changes in the XPS spectrum are also observed; the metallic Ni signal located at 870.2 eV disappeared while the signal at 853 eV became smaller after OER; a similar phenomenon is also observed for the Fe 2p and Mo 3d spectrum; the metallic Fe and Mo signals have almost vanished after OER. All of the results suggest the formation of NiFeMo (oxy)hydroxide on the surface. The NiFe (oxy)hydroxide species have been commonly considered as active OER sites.[67,68] Besides that, as reported by Prof. Cui's group,[69] MoO_x is also active for OER. We believe that self-grown Ni−Fe−Mo (oxy)hydroxides are responsible for the efficient OER activity as well as the high stability of the cell.

In summary, we have demonstrated trimetallic NiFeMo as a highly active electrocatalyst for electrochemical overall water splitting. The trimetallic NiFeMo film serves as a HER catalyst and "precatalyst" for OER. Because of simple synthesis using conventional hydrothermal deposition and thermal annealing, NiFeMo can be easily coated on electrodes such as stainless steel. Unlike most catalysts, the NiFeMo thin film does not require any nanostructuring to be highly active. Together with its high stability, NiFeMo emerges as a great candidate for large-scale commercial application. The catalyst can be coated on other metallic foams such as Cu. Our method can be used to develop active multimetallic catalysts for water splitting, as well as catalysts for oxygen reduction reaction,[70] CO_2 reduction,[71] and methanol oxidation reaction.[72]

■ ASSOCIATED CONTENT

Supporting Information

The Supporting Information is available free of charge on the ACS Publications website at DOI: 10.1021/acsenergylett.7b01335.

Detailed experimental procedures for a trimetallic NiFeMo film on Ni foam and all other controlled samples, additional XRD patterns, XPS spectra, SEM images, EDS mapping images, polarizing curves, TOF calculation process, etc. (PDF)

■ AUTHOR INFORMATION

Corresponding Author

*E-mail: jbao@uh.edu.

ORCID

Zhifeng Ren: 0000-0001-8233-3332

Jiming Bao: 0000-0002-6819-0117

Notes

The authors declare no competing financial interest.

■ ACKNOWLEDGMENTS

J.B. acknowledges support from the Robert A. Welch Foundation (E-1728). Z.Z. thanks support from the National Science Foundation for Postdoctoral Scientists of China (2015M582538). F.R.-H. wishes to thank the FEI (now Thermo Fisher Scientific) team (Dr. D. Gostovic, Dr. L. Pullan, Dr. A. Genc, Dr. L Brock, and Dr. L. Casalena) at the Nanoport facility in Portland for facilitating the FIB (by Dr. L. Brock) and HRTEM (by Dr. A. Genc) observations.

■ REFERENCES

(1) Seh, Z. W.; Kibsgaard, J.; Dickens, C. F.; Chorkendorff, I.; Norskov, J. K.; Jaramillo, T. F. Combining theory and experiment in electrocatalysis: Insights into materials design. *Science* **2017**, *355*, eaad4998.

(2) Sun, K.; Liu, R.; Chen, Y.; Verlage, E.; Lewis, N. S.; Xiang, C. A Stabilized, Intrinsically Safe, 10% Efficient, Solar-Driven Water-Splitting Cell Incorporating Earth-Abundant Electrocatalysts with Steady-State pH Gradients and Product Separation Enabled by a Bipolar Membrane. *Adv. Energy Mater.* **2016**, *6*, 1600379−1600386.

(3) Selopal, G. S.; Zhao, H.; Tong, X.; Benetti, D.; Navarro-Pardo, F.; Zhou, Y.; Barba, D.; Vidal, F.; Wang, Z. M.; Rosei, F. Highly Stable Colloidal "Giant" Quantum Dots Sensitized Solar Cells. *Adv. Funct. Mater.* **2017**, *27*, 1701468−1701482.

(4) Zou, X.; Zhang, Y. Noble metal-free hydrogen evolution catalysts for water splitting. *Chem. Soc. Rev.* **2015**, *44*, 5148−5180.

(5) Suen, N.-T.; Hung, S.-F.; Quan, Q.; Zhang, N.; Xu, Y.-J.; Chen, H. M. Electrocatalysis for the oxygen evolution reaction: recent development and future perspectives. *Chem. Soc. Rev.* **2017**, *46*, 337−365.

(6) Luo, J.; Im, J.-H.; Mayer, M. T.; Schreier, M.; Nazeeruddin, M. K.; Park, N.-G.; Tilley, S. D.; Fan, H. J.; Grätzel, M. Water photolysis at 12.3% efficiency via perovskite photovoltaics and Earth-abundant catalysts. *Science* **2014**, *345*, 1593−1596.

(7) Lv, J. J.; Zhao, J.; Fang, H.; Jiang, L. P.; Li, L. L.; Ma, J.; Zhu, J. J. Incorporating Nitrogen-Doped Graphene Quantum Dots and Ni_3S_2 Nanosheets: A Synergistic Electrocatalyst with Highly Enhanced Activity for Overall Water Splitting. *Small* **2017**, *13*, 1700264.

(8) Li, W.; Gao, X.; Xiong, D.; Wei, F.; Song, W.-G.; Xu, J.; Liu, L. Hydrothermal Synthesis of Monolithic Co_3Se_4 Nanowire Electrodes for Oxygen Evolution and Overall Water Splitting with High Efficiency and Extraordinary Catalytic Stability. *Adv. Energy Mater.* **2017**, *7*, 1602579−1602586.

(9) Tang, C.; Cheng, N.; Pu, Z.; Xing, W.; Sun, X. NiSe Nanowire Film Supported on Nickel Foam: An Efficient and Stable 3D Bifunctional Electrode for Full Water Splitting. *Angew. Chem., Int. Ed.* **2015**, *54*, 9351−9355.

(10) Li, J.; Yan, M.; Zhou, X.; Huang, Z.-Q.; Xia, Z.; Chang, C.-R.; Ma, Y.; Qu, Y. Mechanistic Insights on Ternary $Ni_{2-x}Co_xP$ for Hydrogen Evolution and Their Hybrids with Graphene as Highly Efficient and Robust Catalysts for Overall Water Splitting. *Adv. Funct. Mater.* **2016**, *26*, 6785−6796.

(11) Tan, Y.; Wang, H.; Liu, P.; Shen, Y.; Cheng, C.; Hirata, A.; Fujita, T.; Tang, Z.; Chen, M. Versatile nanoporous bimetallic phosphides towards electrochemical water splitting. *Energy Environ. Sci.* **2016**, *9*, 2257−2261.

(12) Du, C.; Yang, L.; Yang, F.; Cheng, G.; Luo, W. Nest-like NiCoP for Highly Efficient Overall Water Splitting. *ACS Catal.* **2017**, *7*, 4131−4137.

(13) Yu, L.; Zhou, H.; Sun, J.; Qin, F.; Yu, F.; Bao, J.; Yu, Y.; Chen, S.; Ren, Z. Cu nanowires shelled with NiFe layered double hydroxide nanosheets as bifunctional electrocatalysts for overall water splitting. *Energy Environ. Sci.* **2017**, *10*, 1820−1827.

(14) Zhao, Z.; Schipper, D. E.; Leitner, A. P.; Thirumalai, H.; Chen, J.-H.; Xie, L.; Qin, F.; Alam, M. K.; Grabow, L. C.; Chen, S.; et al. Bifunctional metal phosphide FeMnP films from single source metal organic chemical vapor deposition for efficient overall water splitting. *Nano Energy* **2017**, *39*, 444−453.

(15) Duan, J.; Chen, S.; Zhao, C. Ultrathin metal-organic framework array for efficient electrocatalytic water splitting. *Nat. Commun.* **2017**, *8*, 15341−15348.

DOI: 10.1021/acsenergylett.7b01335
ACS Energy Lett. 2018, 3, 546−554

(16) Li, H.; Wen, P.; Li, Q.; Dun, C.; Xing, J.; Lu, C.; Adhikari, S.; Jiang, L.; Carroll, D. L.; Geyer, S. M. Earth-Abundant Iron Diboride (FeB_2) nanoparticles as Highly Active Bifunctional Electrocatalysts for Overall Water Splitting. *Adv. Energy Mater.* **2017**, *7*, 1700513−1700525.
(17) Yu, J.; Li, Q. Q.; Li, Y.; Xu, C. Y.; Zhen, L.; Dravid, V. P.; Wu, J. S. Ternary Metal Phosphide with Triple-Layered Structure as a Low-Cost and Efficient Electrocatalyst for Bifunctional Water Splitting. *Adv. Funct. Mater.* **2016**, *26*, 7644−7651.
(18) Jin, Y.; Yue, X.; Shu, C.; Huang, S.; Shen, P. K. Three-dimensional porous $MoNi_4$ networks constructed by nanosheets as bifunctional electrocatalysts for overall water splitting. *J. Mater. Chem. A* **2017**, *5*, 2508−2513.
(19) Huang, H.; Yu, C.; Zhao, C.; Han, X.; Yang, J.; Liu, Z.; Li, S.; Zhang, M.; Qiu, J. Iron-tuned super nickel phosphide microstructures with high activity for electrochemical overall water splitting. *Nano Energy* **2017**, *34*, 472−480.
(20) Zhang, Y.; Shao, Q.; Pi, Y.; Guo, J.; Huang, X. A Cost-Efficient Bifunctional Ultrathin Nanosheets Array for Electrochemical Overall Water Splitting. *Small* **2017**, *13*, 1700355−1700362.
(21) Liu, J.; Wang, J.; Zhang, B.; Ruan, Y.; Lv, L.; Ji, X.; Xu, K.; Miao, L.; Jiang, J. Hierarchical $NiCo_2S_4$@NiFe LDH Heterostructures Supported on Nickel Foam for Enhanced Overall-Water-Splitting Activity. *ACS Appl. Mater. Interfaces* **2017**, *9*, 15364−15372.
(22) Huang, S.; Meng, Y.; He, S.; Goswami, A.; Wu, Q.; Li, J.; Tong, S.; Asefa, T.; Wu, M. N-, O-, and S-Tridoped Carbon-Encapsulated Co_9S_8 Nanomaterials: Efficient Bifunctional Electrocatalysts for Overall Water Splitting. *Adv. Funct. Mater.* **2017**, *27*, 1606585−1606595.
(23) Zhao, S.; Huang, J.; Liu, Y.; Shen, J.; Wang, H.; Yang, X.; Zhu, Y.; Li, C. Multimetallic Ni-Mo/Cu nanowires as nonprecious and efficient full water splitting catalyst. *J. Mater. Chem. A* **2017**, *5*, 4207−4214.
(24) Stern, L.-A.; Feng, L.; Song, F.; Hu, X. Ni_2P as a Janus catalyst for water splitting: the oxygen evolution activity of Ni_2P nanoparticles. *Energy Environ. Sci.* **2015**, *8*, 2347−2351.
(25) Tian, J.; Cheng, N.; Liu, Q.; Sun, X.; He, Y.; Asiri, A. M. Self-supported NiMo hollow nanorod array: an efficient 3D bifunctional catalytic electrode for overall water splitting. *J. Mater. Chem. A* **2015**, *3*, 20056−20059.
(26) Sivanantham, A.; Ganesan, P.; Shanmugam, S. Hierarchical $NiCo_2S_4$ Nanowire Arrays Supported on Ni Foam: An Efficient and Durable Bifunctional Electrocatalyst for Oxygen and Hydrogen Evolution Reactions. *Adv. Funct. Mater.* **2016**, *26*, 4661−4672.
(27) Wang, Z.; Zeng, S.; Liu, W.; Wang, X.; Li, Q.; Zhao, Z.; Geng, F. Coupling Molecularly Ultrathin Sheets of NiFe-Layered Double Hydroxide on $NiCo_2O_4$ Nanowire Arrays for Highly Efficient Overall Water-Splitting Activity. *ACS Appl. Mater. Interfaces* **2017**, *9*, 1488−1495.
(28) Lewis, N. S. Research opportunities to advance solar energy utilization. *Science* **2016**, *351*, aad1920.
(29) McKone, J. R.; Sadtler, B. F.; Werlang, C. A.; Lewis, N. S.; Gray, H. B. Ni−Mo Nanopowders for Efficient Electrochemical Hydrogen Evolution. *ACS Catal.* **2013**, *3*, 166−169.
(30) Qu, Y.; Medina, H.; Wang, S.-W.; Wang, Y.-C.; Chen, C.-W.; Su, T.-Y.; Manikandan, A.; Wang, K.; Shih, Y.-C.; Chang, J.-W.; et al. Wafer Scale Phase-Engineered 1T- and 2H-$MoSe_2$/Mo Core−Shell 3D-Hierarchical Nanostructures toward Efficient Electrocatalytic Hydrogen Evolution Reaction. *Adv. Mater.* **2016**, *28*, 9658−9658.
(31) Xue, Z.-H.; Su, H.; Yu, Q.-Y.; Zhang, B.; Wang, H.-H.; Li, X.-H.; Chen, J.-S. Janus Co/CoP Nanoparticles as Efficient Mott−Schottky Electrocatalysts for Overall Water Splitting in Wide pH Range. *Adv. Energy Mater.* **2017**, *7*, 1602355−1602362.
(32) Zhang, J.; Wang, T.; Pohl, D.; Rellinghaus, B.; Dong, R.; Liu, S.; Zhuang, X.; Feng, X. Interface Engineering of MoS_2/Ni_3S_2 Heterostructures for Highly Enhanced Electrochemical Overall-Water-Splitting Activity. *Angew. Chem., Int. Ed.* **2016**, *55*, 6702−6707.
(33) Cui, Z.; Ge, Y.; Chu, H.; Baines, R.; Dong, P.; Tang, J.; Yang, Y.; Ajayan, P. M.; Ye, M.; Shen, J. Controlled synthesis of Mo-doped Ni_3S_2 nano-rods: an efficient and stable electro-catalyst for water splitting. *J. Mater. Chem. A* **2017**, *5*, 1595−1602.
(34) Jin, S. Are Metal Chalcogenides, Nitrides, and Phosphides Oxygen Evolution Catalysts or Bifunctional Catalysts? *ACS Energy Lett.* **2017**, *2*, 1937−1938.
(35) Arul Raj, I.; Venkatesan, V. K. Characterization of nickel-molybdenum and nickel-molybdenum-iron alloy coatings as cathodes for alkaline water electrolysers. *Int. J. Hydrogen Energy* **1988**, *13*, 215−223.
(36) Arul Raj, I. Nickel based composite electrolytic surface coatings as electrocatalysts for the cathodes in the energy efficient industrial production of hydrogen from alkaline water electrolytic cells. *Int. J. Hydrogen Energy* **1992**, *17*, 413−421.
(37) Hu, W.; Zhang, Y.; Song, D.; Zhou, Z.; Wang, Y. Electrode properties of amorphous nickel-iron-molybdenum alloy as a hydrogen electrocatalyst in alkaline solution. *Mater. Chem. Phys.* **1995**, *41*, 141−145.
(38) Crnkovic, F. C.; Machado, S. A. S.; Avaca, L. A. Electrochemical and morphological studies of electrodeposited Ni−Fe−Mo−Zn alloys tailored for water electrolysis. *Int. J. Hydrogen Energy* **2004**, *29*, 249−254.
(39) Jeremiasse, A. W.; Bergsma, J.; Kleijn, J. M.; Saakes, M.; Buisman, C. J. N.; Cohen Stuart, M.; Hamelers, H. V. M. Performance of metal alloys as hydrogen evolution reaction catalysts in a microbial electrolysis cell. *Int. J. Hydrogen Energy* **2011**, *36*, 10482−10489.
(40) Jayalakshmi, W.-Y. K. M.; Kwang-Deog Jung; Oh-Shim Joo. Electrochemical Characterization of Ni-Mo-Fe Composite Film in Alkali Solution. *Int. J. Electrochem. Sci.* **2008**, *3*, 908−917.
(41) Han, N.; Zhao, F.; Li, Y. Ultrathin nickel-iron layered double hydroxide nanosheets intercalated with molybdate anions for electrocatalytic water oxidation. *J. Mater. Chem. A* **2015**, *3*, 16348−16353.
(42) Xie, C.; Wang, Y.; Hu, K.; Tao, L.; Huang, X.; Huo, J.; Wang, S. In situ confined synthesis of molybdenum oxide decorated nickel-iron alloy nanosheets from MoO_4^{2-} intercalated layered double hydroxides for the oxygen evolution reaction. *J. Mater. Chem. A* **2017**, *5*, 87−91.
(43) McCrory, C. C. L.; Jung, S.; Ferrer, I. M.; Chatman, S. M.; Peters, J. C.; Jaramillo, T. F. Benchmarking Hydrogen Evolving Reaction and Oxygen Evolving Reaction Electrocatalysts for Solar Water Splitting Devices. *J. Am. Chem. Soc.* **2015**, *137*, 4347−4357.
(44) Jamesh, M. I. Recent progress on earth abundant hydrogen evolution reaction and oxygen evolution reaction bifunctional electrocatalyst for overall water splitting in alkaline media. *J. Power Sources* **2016**, *333*, 213−236.
(45) Peng, S. J.; Li, L. L.; Wu, H. B.; Madhavi, S.; Lou, X. W. Controlled Growth of $NiMoO_4$ Nanosheet and Nanorod Arrays on Various Conductive Substrates as Advanced Electrodes for Asymmetric Supercapacitors. *Adv. Energy Mater.* **2015**, *5*, 1401172−1401179.
(46) Merki, D.; Vrubel, H.; Rovelli, L.; Fierro, S.; Hu, X. Fe, Co, and Ni ions promote the catalytic activity of amorphous molybdenum sulfide films for hydrogen evolution. *Chem. Sci.* **2012**, *3*, 2515−2525.
(47) Popczun, E. J.; McKone, J. R.; Read, C. G.; Biacchi, A. J.; Wiltrout, A. M.; Lewis, N. S.; Schaak, R. E. Nanostructured Nickel Phosphide as an Electrocatalyst for the Hydrogen Evolution Reaction. *J. Am. Chem. Soc.* **2013**, *135*, 9267−9270.
(48) Duan, J.; Chen, S.; Vasileff, A.; Qiao, S. Z. Anion and Cation Modulation in Metal Compounds for Bifunctional Overall Water Splitting. *ACS Nano* **2016**, *10*, 8738−8745.
(49) Jia, X. D.; Zhao, Y. F.; Chen, G. B.; Shang, L.; Shi, R.; Kang, X. F.; Waterhouse, G. I. N.; Wu, L. Z.; Tung, C. H.; Zhang, T. R. Ni_3FeN Nanoparticles Derived from Ultrathin NiFe-Layered Double Hydroxide Nanosheets: An Efficient Overall Water Splitting Electrocatalyst. *Adv. Energy Mater.* **2016**, *6*, 1502585−1502591.
(50) Hu, F.; Zhu, S.; Chen, S.; Li, Y.; Ma, L.; Wu, T.; Zhang, Y.; Wang, C.; Liu, C.; Yang, X.; et al. Amorphous Metallic NiFeP: A Conductive Bulk Material Achieving High Activity for Oxygen Evolution Reaction in Both Alkaline and Acidic Media. *Adv. Mater.* **2017**, *29*, 1606570−1606579.

DOI: 10.1021/acsenergylett.7b01335
ACS Energy Lett. 2018, 3, 546−554

(51) Jia, Y.; Zhang, L.; Gao, G.; Chen, H.; Wang, B.; Zhou, J.; Soo, M. T.; Hong, M.; Yan, X.; Qian, G.; et al. A Heterostructure Coupling of Exfoliated Ni-Fe Hydroxide Nanosheet and Defective Graphene as a Bifunctional Electrocatalyst for Overall Water Splitting. *Adv. Mater.* **2017**, *29*, 1700017−1700025.
(52) Xu, Y.; Tu, W.; Zhang, B.; Yin, S.; Huang, Y.; Kraft, M.; Xu, R. Nickel Nanoparticles Encapsulated in Few-Layer Nitrogen-Doped Graphene Derived from Metal-Organic Frameworks as Efficient Bifunctional Electrocatalysts for Overall Water Splitting. *Adv. Mater.* **2017**, *29*, 1605957−1605965.
(53) Gong, M.; Li, Y.; Wang, H.; Liang, Y.; Wu, J. Z.; Zhou, J.; Wang, J.; Regier, T.; Wei, F.; Dai, H. An Advanced Ni−Fe Layered Double Hydroxide Electrocatalyst for Water Oxidation. *J. Am. Chem. Soc.* **2013**, *135*, 8452−8455.
(54) Stevens, M. B.; Enman, L. J.; Batchellor, A. S.; Cosby, M. R.; Vise, A. E.; Trang, C. D. M.; Boettcher, S. W. Measurement Techniques for the Study of Thin Film Heterogeneous Water Oxidation Electrocatalysts. *Chem. Mater.* **2017**, *29*, 120−140.
(55) Jung, S.; McCrory, C. C. L.; Ferrer, I. M.; Peters, J. C.; Jaramillo, T. F. Benchmarking nanoparticulate metal oxide electrocatalysts for the alkaline water oxidation reaction. *J. Mater. Chem. A* **2016**, *4*, 3068−3076.
(56) Klingan, K.; Ringleb, F.; Zaharieva, I.; Heidkamp, J.; Chernev, P.; Gonzalez-Flores, D.; Risch, M.; Fischer, A.; Dau, H. Water Oxidation by Amorphous Cobalt-Based Oxides: Volume Activity and Proton Transfer to Electrolyte Bases. *ChemSusChem* **2014**, *7*, 1301−1310.
(57) Doyle, R. L.; Godwin, I. J.; Brandon, M. P.; Lyons, M. E. G. Redox and electrochemical water splitting catalytic properties of hydrated metal oxide modified electrodes. *Phys. Chem. Chem. Phys.* **2013**, *15*, 13737−13783.
(58) Yang, Y.; Zhang, K.; Lin, H.; Li, X.; Chan, H. C.; Yang, L.; Gao, Q. MoS_2−Ni_3S_2 Heteronanorods as Efficient and Stable Bifunctional Electrocatalysts for Overall Water Splitting. *ACS Catal.* **2017**, *7*, 2357−2366.
(59) Wu, Y.; Li, G.-D.; Liu, Y.; Yang, L.; Lian, X.; Asefa, T.; Zou, X. Overall Water Splitting Catalyzed Efficiently by an Ultrathin Nanosheet-Built, Hollow Ni_3S_2-Based Electrocatalyst. *Adv. Funct. Mater.* **2016**, *26*, 4839−4847.
(60) Chen, P.; Zhou, T.; Zhang, M.; Tong, Y.; Zhong, C.; Zhang, N.; Zhang, L.; Wu, C.; Xie, Y. 3D Nitrogen-Anion-Decorated Nickel Sulfides for Highly Efficient Overall Water Splitting. *Adv. Mater.* **2017**, *29*, 1701584−1701590.
(61) You, B.; Jiang, N.; Sheng, M.; Bhushan, M. W.; Sun, Y. Hierarchically Porous Urchin-Like Ni_2P Superstructures Supported on Nickel Foam as Efficient Bifunctional Electrocatalysts for Overall Water Splitting. *ACS Catal.* **2016**, *6*, 714−721.
(62) Liu, Y.; Li, Q.; Si, R.; Li, G.-D.; Li, W.; Liu, D.-P.; Wang, D.; Sun, L.; Zhang, Y.; Zou, X. Coupling Sub-Nanometric Copper Clusters with Quasi-Amorphous Cobalt Sulfide Yields Efficient and Robust Electrocatalysts for Water Splitting Reaction. *Adv. Mater.* **2017**, *29*, 1606200−1606208.
(63) Yu, Z.-Y.; Duan, Y.; Gao, M.-R.; Lang, C.-C.; Zheng, Y.-R.; Yu, S.-H. A one-dimensional porous carbon-supported Ni/Mo_2C dual catalyst for efficient water splitting. *Chem. Sci.* **2017**, *8*, 968−973.
(64) Yang, Y.; Fei, H.; Ruan, G.; Tour, J. M. Porous Cobalt-Based Thin Film as a Bifunctional Catalyst for Hydrogen Generation and Oxygen Generation. *Adv. Mater.* **2015**, *27*, 3175−3180.
(65) Zeradjanin, A. R.; Grote, J.-P.; Polymeros, G.; Mayrhofer, K. J. J. A Critical Review on Hydrogen Evolution Electrocatalysis: Re-exploring the Volcano-relationship. *Electroanalysis* **2016**, *28*, 2256−2269.
(66) Zhang, Y.; Ouyang, B.; Xu, J.; Chen, S.; Rawat, R. S.; Fan, H. J. 3D Porous Hierarchical Nickel-Molybdenum Nitrides Synthesized by RF Plasma as Highly Active and Stable Hydrogen-Evolution-Reaction Electrocatalysts. *Adv. Energy Mater.* **2016**, *6*, 1600221−1600227.
(67) Liang, H.; Gandi, A. N.; Xia, C.; Hedhili, M. N.; Anjum, D. H.; Schwingenschlögl, U.; Alshareef, H. N. Amorphous NiFe-OH/NiFeP Electrocatalyst Fabricated at Low Temperature for Water Oxidation Applications. *ACS Energy Lett.* **2017**, *2*, 1035−1042.
(68) Wang, A.-L.; Xu, H.; Li, G.-R. NiCoFe Layered Triple Hydroxides with Porous Structures as High-Performance Electrocatalysts for Overall Water Splitting. *ACS Energy Lett.* **2016**, *1*, 445−453.
(69) Jin, Y.; Wang, H.; Li, J.; Yue, X.; Han, Y.; Shen, P. K.; Cui, Y. Porous MoO_2 Nanosheets as Non-noble Bifunctional Electrocatalysts for Overall Water Splitting. *Adv. Mater.* **2016**, *28*, 3785−3790.
(70) Jiang, K.; Zhao, D.; Guo, S.; Zhang, X.; Zhu, X.; Guo, J.; Lu, G.; Huang, X. Efficient oxygen reduction catalysis by subnanometer Pt alloy nanowires. *Sci. Adv.* **2017**, *3*, e1601705.
(71) Luc, W.; Collins, C.; Wang, S.; Xin, H.; He, K.; Kang, Y.; Jiao, F. Ag−Sn Bimetallic Catalyst with a Core−Shell Structure for CO_2 Reduction. *J. Am. Chem. Soc.* **2017**, *139*, 1885−1893.
(72) Cui, X.; Xiao, P.; Wang, J.; Zhou, M.; Guo, W.; Yang, Y.; He, Y.; Wang, Z.; Yang, Y.; Zhang, Y.; et al. Highly Branched Metal Alloy Networks with Superior Activities for the Methanol Oxidation Reaction. *Angew. Chem.* **2017**, *129*, 4559−4564.

DOI: 10.1021/acsenergylett.7b01335
ACS Energy Lett. 2018, 3, 546−554